Mechanical Systems and Signal Processing 202 (2023) 110656

Contents lists available at ScienceDirect

Mechanical Systems and Signal Processing

journal homepage: www.elsevier.com/locate/ymssp

Minimum detectable changes based on linear Bayesian filters

Francesca Marsili [a,*], Alexander Mendler [b], Filippo Landi [c], Sylvia Kessler [a]

[a] Helmut-Schmidt-University/ University of the Federal Armed Forces, Chair of Engineering Materials and Building Preservation, PO box 700822, 22008 Hamburg, Germany

[b] Technical University of Munich, TUM School of Engineering and Design, Department of Materials Engineering, Chair of Non-destructive Testing, Franz-Langinger-Str 10, 81245 Munich, Germany

[c] University of Pisa, Department of Civil and Industrial Engineering, Largo Lucio Lazzarino, 56122 Pisa, Italy

ARTICLE INFO

Communicated by M. Beer

Keywords:
Structural health monitoring
Model updating
Detectability
Bayesian inverse problem
Kalman filter
Polynomial chaos expansion
Uncertainty quantification

ABSTRACT

This article proposes a method to assess the minimum detectable changes in system parameters based on Bayesian inference. The approach considers the monitored parameters as random variables, and uses linear Bayesian filters to update them based on system observations. To determine the detectable changes in them, a special quality of Kalman filter is exploited, that is, the fact that the posterior variance is independent of the observations of the changed state, and that it can be calculated based on previous knowledge. To enable an automated change diagnosis, a decision rule is introduced, based on the posterior's probability of exceeding a user-defined threshold. This way, the user can specify an allowable probability of exceedance, and subsequently, this value can be converted into an equivalent detectable change. To cope with large systems and multiple system observations, a functional Kalman Filter is applied, which enables an analytical solution to the Bayesian inverse problem. For proof of concept, three numerical case studies related to structural health monitoring are presented, including a 6-DOF mass-and-spring system, an offshore tower subject to marine growth, and a reinforced concrete bridge affected by seismic damage. The case studies highlight that no data from the changed state is required to accurately evaluate the detectable change. Secondly, the detectability can be evaluated for any measurement quantity (vibrations, inclinations) or extracted damage-sensitive feature (natural frequencies, mode shapes), provided it is sensitive to changes in the system parameters. Furthermore, the detectability can be assessed for various damage scenarios and a wide range of monitored systems, provided that numerical models are available, e.g. physics-based models or surrogate models.

1. Introduction

Bayesian methods are suitable tools to solve inverse problems, that is, to analyze the observable system outputs through sensors, and to infer knowledge on latent system inputs that caused the changes in data. They consider previous knowledge on the system parameters (through the prior) as well as the uncertainties in the measurements (through the likelihood) to infer an updated system parameter (the posterior). Traditionally, the magnitude of changes is assessed a posteriori, that is, based on data in the changed state, and a change diagnosis is issued by comparing the posterior to a safety threshold. However, in some cases, it might be desirable to assess the change detectability before this data becomes available, for example, to assess the performance of the measuring system and to convince the system operators of the added value. On this background, the objective of this article is to develop a method to "predictively" assess the detectable parameter changes.

* Corresponding author.
E-mail address: francesca.marsili@hsu-hh.de (F. Marsili).

https://doi.org/10.1016/j.ymssp.2023.110656
Received 22 February 2023; Received in revised form 31 May 2023; Accepted 31 July 2023
Available online 18 August 2023

The problem statement is motivated by structural health monitoring (SHM) applications with large and expensive engineering structures, such as, bridges, highrises, dams, and power plants. Due to their uniqueness, no data is available from the damage states, and damages may evolve over long time periods. Yet, it is important to know what a monitoring system can achieve before it is implemented. The diagnosis procedure is typically divided into multiple steps: the acquisition of measurements, the extraction of damage-sensitive features, and their statistical evaluation [1]. The diagnostic depth can be categorized into four hierarchical steps of increasing complexity, e.g. damage detection, localization, quantification, and lifetime prediction [2]. For each step, it is important to clearly communicate the reliability of the automated monitoring system, and one way of doing this is by determining the diagnosable damages, i.e., the detectable changes in the structure that the monitoring system can sense based on uncertain measurements. Various approaches exists in the literature for this purpose, but most of them are empirical, structure-specific, and cannot be transferred to other structures. For example, Coppolino et al. [3] developed a structure-specific rule of thumb for offshore structures, and estimates how many frame members have to fail for these structural changes to become observable in ambient vibration data. Other approaches resort to synthetically generated data to assess the detectability, e.g. for masonry bell towers [4,5], but simulated time histories often fail to accurately capture the distribution properties of non-stationary excitation and measurement noise (Gaussian vs. uniform, white noise vs. colored noise). The accurate quantification of measurement errors is critical to assess the detectability of damage, and therefore, a common approach is to compare the deviations to their 95% confidence bounds [6]. Alternatively, one can resort to well-established methods to evaluate the probability of detection (POD), i.e., the probability that a change in a material, component, or system is detected, given that it is present. According to design standards in non-destructive testing [7–9], the POD can be evaluated as the relative number of signals beyond a user-defined threshold, but this requires destructive tests on 30 to 90 specimens, which are not feasible for bridges, dams, or other SHM applications.

On this background, Mendler et al. [10] developed a "predictive" method to calculate the POD based on data from undamaged structures, and this method is universally applicable to any structure that can be modeled through analytical formulas. The prediction requires knowledge on the physical relation between system inputs and observable outputs (captured in a sensitivity matrix) and it is only accurate for small structural changes due to a first-order Taylor expansion. Mendler et al. [11] expanded the framework to predict the minimum localizable damage, and concluded that defining the optimal localizability is a multi-objective optimization problem, as an increased localization resolution leads to a smaller detectability, and more frequent alarms in unchanged components, due to the numerical ill-conditioning of inverse problems. All presented approaches assume deterministic input parameters, but this assumption may not be justified for system inputs with large uncertainties. Bayesian methods [12], on the other hand, treat system parameters as random variables and provide advanced diagnostic capabilities, such as, damage quantification [13] and the prediction of the remaining lifetime [14]. Commonly, the changed state is distinguished from the unchanged state through user-defined safety thresholds as well, and the region between the upper and lower control limits is sometimes called the region of practical equivalence [15]. A common way to solve inverse problem based on Bayesian inference is Markov Chain Monte Carlo (MCMC) sampling, but this method can be time-consuming, and might fail to update SHM models due to the large number of parameters and observations. To remedy this, more efficient approaches have been developed to solve Bayesian inverse problem based on functional approximation of random variables [16–19] with successful applications in non-destructive testing (NDT) and SHM [20–23]. A particularly interesting method is the Kalman filter based on polynomial chaos expansion (PCE) [24,25], as it analytically solves the inverse problem, and can handle a large number of observations and system parameters. The method was applied to parameter identification [26,27] as well as damage assessment [28,29], but the reliability of the diagnosis was never explicitly considered.

The objective of this paper is to develop a fully-probabilistic framework to assess the minimum detectable changes before damage occurs. For this purpose, linear Bayesian filters are employed to "predict" the uncertainty affecting the parameter, and to compare it against the user-defined thresholds for damage quantification. To deal with large engineering problems and slightly non-linear systems, a PCE-based Kalman filter is incorporated that can handle a large number of observations and system parameters. The method considers the uncertainties in the system parameters and in the observations, and three approaches are recapped to quantify the measurement errors. The paper is organized as follows: Section 2 gives some background on Bayesian model updating using Kalman filters and general polynomial chaos expansion. Moreover, a simplified numerical study is introduced, which is used throughout this paper to highlight the new developments. Section 3 introduces the concept of damage detectability for Bayesian updating. In Section 4, the method is applied in two numerical proof of concept studies, and Section 5 draws some conclusions.

2. Bayesian model updating

2.1. Bayesian inverse problems

Let us consider a mechanical system whose dynamic behavior can be modeled through a set of partial differential equations. The model is characterized by a system input vector $\mathbf{Q} \in \mathbb{R}^{N_p}$ with N_p parameters. In this paper, the inputs are modeled as Gaussian independent variables

$$\mathbf{Q} \sim \mathcal{N}(\boldsymbol{\mu}_Q, \mathbf{C}_Q), \tag{1}$$

so they can be uniquely described through one mean vector $\boldsymbol{\mu}_Q \in \mathbb{R}^{N_p}$ and a diagonal covariance matrix $\mathbf{C}_Q \in \mathbb{R}^{N_p \times N_p}$. In this paper, capital latin letters $\mathbf{Q}$ are used for random variables and small $\mathbf{q}$ letters for their realizations. A deterministic mechanical system G is assumed that transforms the system inputs $\mathbf{Q}$ into the outputs $\mathbf{y} = G(\mathbf{q}) \in \mathbb{R}^{N_f}$, where N_f is the number of observations. Since measurement errors are inevitable in practice due to noisy sensors or uncertainties in the feature estimation process, the

observable output $\mathbf{z}$ is modeled as a linear superposition of the observations and the error, i.e., $\mathbf{Z} = G(\mathbf{Q}) + \mathbf{E}$. The distribution of the measurement error $\mathbf{E} \in \mathbb{R}^{N_f}$ itself,

$$\mathbf{E} = \mathbf{Z} - G(\mathbf{Q}) \sim \mathcal{N}(\mathbf{0}, \mathbf{C}_E), \tag{2}$$

is assumed to have a zero mean vector and a diagonal covariance matrix $\mathbf{C}_E \in \mathbb{R}^{N_f \times N_f}$. The Bayesian approach seeks to estimate the random vector $\mathbf{Q}$ given a single observation $\mathbf{z}$. After updating, the posterior random variable $\mathbf{Q}'$ can be written as

$$\pi_{\mathbf{Q}'}(\mathbf{q}) = \frac{L(\mathbf{q})\pi_Q(\mathbf{q})}{\int L(\mathbf{q})\pi_Q(\mathbf{q})dq}, \qquad L(\mathbf{q}) = \prod_{i=1}^{N_f} \pi_{E_i}(z_i - y_i), \tag{3}$$

where π describes the probability density function (PDF) and $L(\mathbf{q})$ is the likelihood function. In most cases, the likelihood and the posterior distribution cannot be analytically derived in closed form. A common approach to circumvent this problem is MCMC sampling, but it can be computationally demanding. More efficient approaches are outlined in the next sections.

2.2. Linear Bayesian filters

An efficient approach to Bayesian updating is the calibration of statistical moments instead of entire PDFs. Following the derivation in Litvinenko and Matthies [30], one may rewrite the Bayes rule in terms of a quadratic minimization problem and, by restricting the solution to the linear measurable functions, obtain the linear Bayesian formula

$$\mathbf{Q}' = \mathbf{Q} + \mathbf{K}(\mathbf{z} - \mathbf{Y}), \tag{4}$$

where $\mathbf{Q}$ is the prior, $\mathbf{z}$ are the observations, and $\mathbf{Y}$ are system outputs from a analytical model. The metric $\mathbf{K}$ is the Kalman gain [31]

$$\mathbf{K} = \mathbf{C}_{\mathbf{QY}} \left[\mathbf{C}_{\mathbf{Y}} + \mathbf{C}_{\mathbf{E}}\right]^{-1}, \tag{5}$$

where $\mathbf{C}_{\mathbf{Y}}$ is the system output covariance, $\mathbf{C}_{\mathbf{E}}$ is the error covariance, and $\mathbf{C}_{\mathbf{QY}}$ is the covariance between the system inputs and the system outputs. If the prior $\mathbf{Q}$ is Gaussian as in Eq. (1), and the model G is linear, it can be shown that the posterior is Gaussian as well $\mathbf{Q}' \sim \mathcal{N}(\boldsymbol{\mu}_{\mathbf{Q}'}, \mathbf{C}_{\mathbf{Q}'})$, with the mean and the covariance [32]

$$\boldsymbol{\mu}_{\mathbf{Q}'} = \boldsymbol{\mu}_{\mathbf{Q}} + \mathbf{K}(\mathbf{z} - \mathrm{G}(\boldsymbol{\mu}_{\mathbf{Q}})), \qquad \mathbf{C}_{\mathbf{Q}'} = \mathbf{C}_{\mathbf{Q}} - \mathbf{K}\mathbf{C}_{\mathbf{QY}}^T. \tag{6}$$

The updated covariance $\mathbf{C}_{\mathbf{Q}'}$ is independent of the observation, and therefore, all quantities for its computation are available based on data from the unchanged system. This fundamental relation will be leveraged in this paper to define the detectable change in input parameters.

2.3. Polynomial chaos expansion

If the model is non-linear, the calculation of the cross-covariance $\mathbf{C}_{\mathbf{QY}}$ is not straightforward. For this reason, the PCE-based Kalman filter is developed, which is suited for slightly non-linear problems with a high number of observations and parameters [33]. The main idea is to represent all random variables in PCE form, and to update the PCE coefficients $\hat{\mathbf{q}}$ based on the linear Bayesian formula. Let us assume that each random variable is represented in PCE form, with a suitable basis, and subsequently transformed into a unified basis [32]

$$\hat{\mathbf{Q}} = \sum_{\mathcal{I}} \hat{\mathbf{q}}_{\boldsymbol{\alpha}} \mathbf{H}_{\boldsymbol{\alpha}}, \quad \hat{\mathbf{Y}} = \sum_{\mathcal{I}} \hat{\mathbf{y}}_{\boldsymbol{\alpha}} \mathbf{H}_{\boldsymbol{\alpha}}, \quad \hat{\mathbf{Z}} = \sum_{\mathcal{I}} \hat{\mathbf{z}}_{\boldsymbol{\alpha}} \mathbf{H}_{\boldsymbol{\alpha}}, \quad \hat{\mathbf{E}} = \sum_{\mathcal{I}} \hat{\mathbf{e}}_{\boldsymbol{\alpha}} \mathbf{H}_{\boldsymbol{\alpha}}, \tag{7}$$

where $\hat{\mathbf{q}}_{\boldsymbol{\alpha}}$, $\hat{\mathbf{y}}_{\boldsymbol{\alpha}}$, $\hat{\mathbf{z}}_{\boldsymbol{\alpha}}$, $\hat{\mathbf{e}}_{\boldsymbol{\alpha}}$ are coefficients and $\hat{\mathbf{H}}_{\boldsymbol{\alpha}}$ represents the generalized multi-variate orthogonal polynomials. Since Gaussian random variables are assumed, Hermite polynomials are used as basis functions [34]. The letter $\mathcal{I}$ represents the set of all finite, non-negative integer sequences, i.e. multi-indices $\boldsymbol{\alpha}$ such that the following expression holds [19]

$$\mathcal{I} := \boldsymbol{\alpha} = (\alpha_1, \ldots, \alpha_j, \ldots) \quad \Big| \quad \alpha_j \in \mathbb{N}_0^{(\mathbb{N})}, \quad |\boldsymbol{\alpha}| = \sum_{j=1}^{\infty} \alpha_j < \infty. \tag{8}$$

For computational efficiency, only a finite subset of $\mathcal{I}$ is taken, and the expansion is truncated after the polynomial order p. In Eq. (7), the variables $\hat{\mathbf{Y}} \in \mathbb{R}^{N_p \times N_f}$, $\hat{\mathbf{Z}} \in \mathbb{R}^{N_p \times N_f}$ represent the system output and the observation, respectively. Various approaches exist to estimate the coefficients, e.g., interpolation, regression, or projection [35], where the latter is used in this paper. In this case, the linear Bayesian updating procedure can be reduced to an analytical method, and Eq. (4) can be rewritten in the following form

$$\hat{\mathbf{Q}}' = \hat{\mathbf{Q}} + \mathbf{K}(\hat{\mathbf{z}} - \hat{\mathbf{Y}}), \tag{9}$$

where $\mathbf{K}$ is the Kalman filter evaluated with the following covariances

$$\mathbf{C}_{\mathbf{Y}} = \sum_{\boldsymbol{\alpha}>0} \boldsymbol{\alpha}! \hat{\mathbf{y}}_{\boldsymbol{\alpha}} (\hat{\mathbf{y}}_{\boldsymbol{\alpha}})^T, \quad \mathbf{C}_{\mathbf{E}} = \sum_{\boldsymbol{\alpha}>0} \boldsymbol{\alpha}! \hat{\mathbf{e}}_{\boldsymbol{\alpha}} (\hat{\mathbf{e}}_{\boldsymbol{\alpha}})^T, \quad \mathbf{C}_{\mathbf{QY}} = \sum_{\boldsymbol{\alpha}>0} \boldsymbol{\alpha}! \hat{\mathbf{q}}_{\boldsymbol{\alpha}} (\hat{\mathbf{y}}_{\boldsymbol{\alpha}})^T. \tag{10}$$

This approach is particularly efficient in comparison to MCMC, because the model G only has to be run a few times to build the PCE-based surrogate model. Moreover, the posterior variance can be estimated analytically based on observations from the unchanged system.

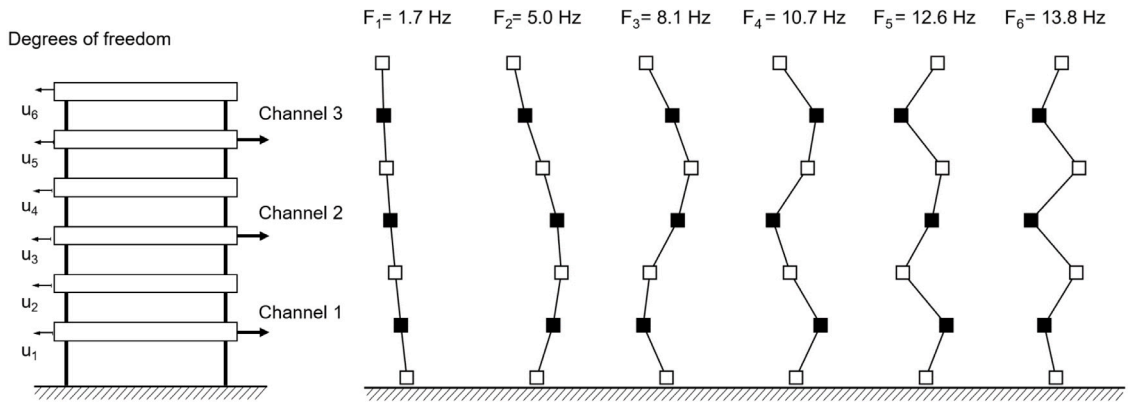

Fig. 1. 6-DOF mass and spring system with deterministic masses $m = 1000$ t and stochastic springs with a mean of $\mu_K = 2000$ MN/m (left) and the corresponding natural frequencies and mode shapes (right).

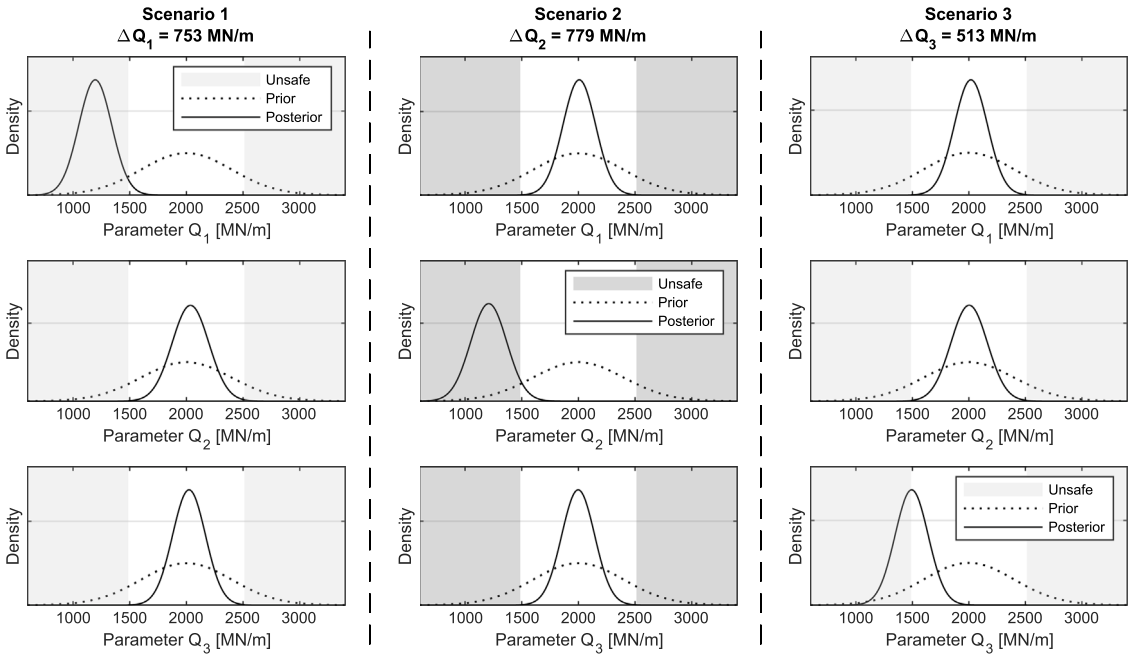

Fig. 2. Damage detection, localization, and quantification result for the 6-DOF system with a stiffness decrease in parameter Q_1 (left), parameter Q_2 (center), and parameter Q_3 (right).

2.4. 6-DOF example

In this section, a case study is introduced to demonstrate how the inverse problem can be solved based on PCE-based Kalman filters and how damage can be quantified in SHM. Note that all case studies in this paper are based on numerical simulations. The structure under consideration is a six-story building with rigid slabs and slender columns, which is simplified to a mass-and-spring system with six horizontal degrees of freedom (DOF) u_1 to u_6 and the properties shown in Fig. 1.

The input parameters to be updated are the three stiffness values of the lower floors $\mathbf{Q} = [K_1, K_2, K_3]$ characterized by a Gaussian distribution with a mean value of 2000 MN/m and a standard deviation of 400 MN/m each. The observed features are the first six natural frequencies $\mathbf{Z} = [F_1 \dots F_6]$. They are calculated based on numerical modal analysis and treated as the mean value of the considered observations. The error covariance $\mathbf{C}_E$ is assumed to be known and fixed by the user to the following values for reproducibility

$$\mathbf{C}_E = \mathrm{diag}\left[0.017^2 \quad 0.051^2 \quad 0.081^2 \quad 0.107^2 \quad 0.126^2 \quad 0.138^2\right], \tag{11}$$

meaning the standard deviation of the error related to the first natural frequency is 0.017. Damage was modeled by individually shifting the mean value of one input parameter at a time, so three damage scenarios can be distinguished. Before solving the inverse

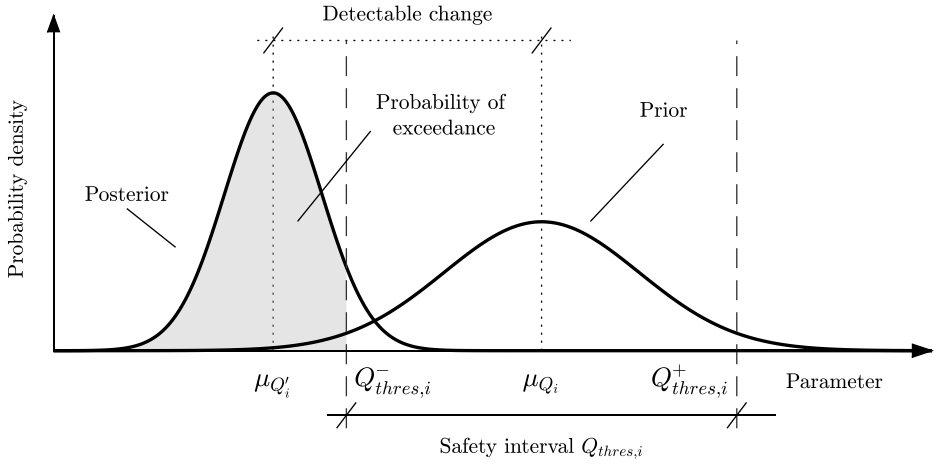

Fig. 3. Distribution of a single parameter Q_i.

problem, a surrogate model based on PCE has to be built. In the first step, the input random parameters are mapped onto a reference set of standard Gaussian variables (the germ). Then, the coefficients are evaluated through projection, and by re-running the model at several integration points, with the result being a surrogate model of the observed system outputs. Subsequently, an "artificial" measurement is generated with both the original finite element model and the surrogate model, and the order p of the expansion is increased until the differences between the two model outputs are negligible. In all case studies in this paper, a polynomial order of $p = 5$ is deemed sufficient. For a detailed description of this procedure, please refer to Friedman et al. [32]. Based on the surrogate model, the covariances and the Kalman filter can be computed, using Eqs. (9) and (10), and the mean value and the standard deviation of the input parameters can be updated based on observations of the system outputs using Eq. (6). Note that no sampling is required in this procedure, as the mean and the variance of the posterior can be computed analytically.

Fig. 2 shows the result from Bayesian updating for all three damage scenarios with damage on the ground floor (left), second floor (center), and the third floor (right). The prior distribution is indicated through a dotted line and the posterior distribution through a solid line. For the first damage scenario (on the left side of the figure), the posterior distribution shifts to the left with a new mean of $\mu_{Q_1'} = 2000 - 753 = 1247$ MN/m, while the posterior distribution of other parameters Q_2 and Q_3 remain unchanged. This way, damage can be detected, localized on the ground floor, and quantified accurately. Comparing the posterior and the prior, it can be appreciated that the spread of the distribution decreases, meaning the uncertainty in the parameter has decreased because additional information is available from measurements. The "true" value for the input parameter is not necessarily at the mean value but anywhere below the density function. Since the posterior extends to infinity, one may ask how far the mean value has to shift, so an automated monitoring system can make a reliable statement regarding the true state of the system parameter. This question is addressed in the subsequent sections, which also give more information on how to determine the safety intervals in Fig. 2.

3. Minimum detectable changes

Bayesian approaches allow for input parameters to be modeled as random variables, and in this paper, they are assumed to be Gaussian, see Fig. 3. The mean and covariance are generally known based on previous knowledge, $\mathbf{Q} \sim \mathcal{N}(\boldsymbol{\mu}_\mathbf{Q}, \mathbf{C}_\mathbf{Q})$. If measurements of system outputs are available, the covariance of the parameter estimates $\mathbf{C}_{\mathbf{Q}'}$ can be updated using Bayesian linear filters, see Eq. (6). It depends on the prior covariance, the measurement error, as well as the covariance between inputs and outputs. This relation will now be leveraged to determine how far the distribution of the system parameter has to shift for a reliable damage diagnosis, and to estimate the minimum detectable damage.

Before the detectability of damages in input parameters can be assessed, the anticipated changes have to be parameterized, i.e., expressed through parameter changes. In all following considerations, system changes are modeled as changes in the mean input vector

$$\Delta\mathbf{Q} = \boldsymbol{\mu}_{\mathbf{Q}'} - \boldsymbol{\mu}_\mathbf{Q}, \tag{12}$$

where $\boldsymbol{\mu}_\mathbf{Q}$ is the mean vector before changes occur and $\boldsymbol{\mu}_{\mathbf{Q}'}$ afterward. Parameter changes can have a positive or negative sign. The true parameters may not coincide with the mean values but lay anywhere within the density functions from Fig. 3. Therefore, a decision rule has to be implemented to enable an automated monitoring system to determine if the parameters have changed. One way to achieve this is to define a safety interval $\mathbf{Q}_{thres} \in \mathbb{R}^{N_p,2}$ by setting a lower and upper threshold $Q^-_{thres,i}$ and $Q^+_{thres,i}$ for each parameter,

$$\mathbf{Q}_{thres} = \begin{bmatrix} \mathbf{Q}^-_{thres} & \mathbf{Q}^+_{thres} \end{bmatrix}, \tag{13}$$

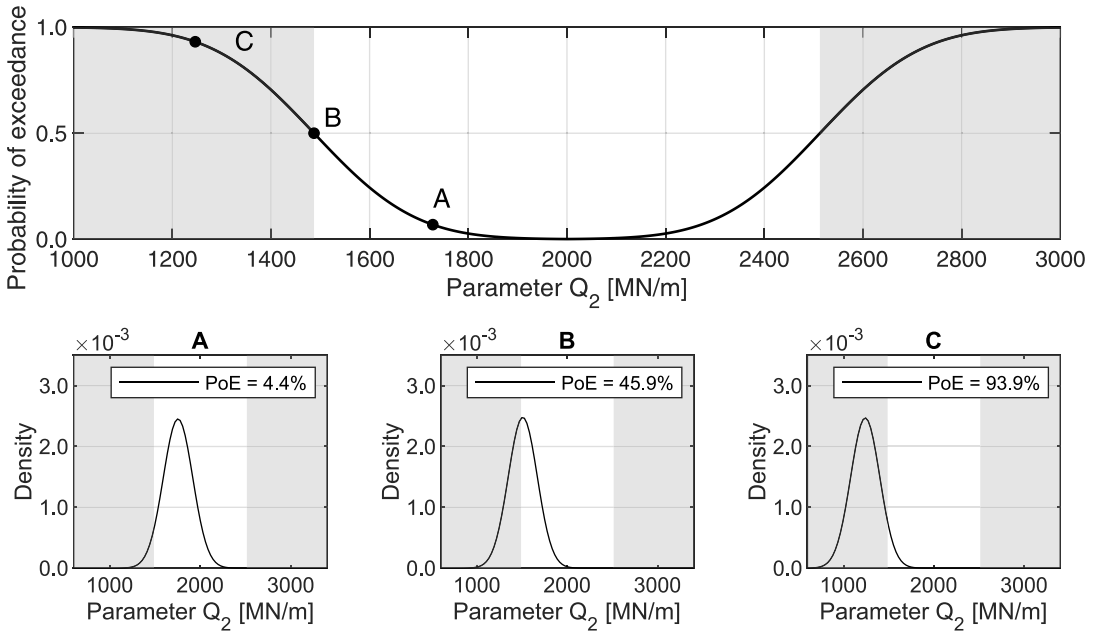

Fig. 4. Probability of exceedance (POE) curve for parameter Q_2 of the 6-DOF system.

and to compare the posterior distributions against the safety thresholds. In many cases, the safety interval can be determined based on engineering knowledge, either based on material-specific strength values that must not be exceeded or based on experience gained from the analysis of similar structures. If this is not possible, the safety threshold could be determined based on national design standards and the target reliability concept. A third option is to define the safety threshold based on the posterior distribution, but more on this follows in Section 3.3.

3.1. Probability of exceedance

This section introduces the decision criterion to automatically determine if the parameters have changed. To ease its explanation, the discussion is focused on a single parameter change ΔQ_i. Safe operation is guaranteed if the true parameter lays within the safety thresholds from Eq. (13). However, the distribution of Q_i extends from zero to infinity, and some proportion of the density function will always be beyond the thresholds, even if no changes have occurred, see Fig. 3. A critical condition arises when the input parameter shifts beyond the safety thresholds, i.e., if it is significantly lower or higher. Even if the mean parameter estimate $\mu_{Q_i'}$ does not move beyond but close to the safety threshold, a significant proportion of the distribution may stretch beyond the thresholds, indicating a possibly critical state. The tail of the distribution beyond the safety threshold describes the likelihood that the parameter is in changed state, which is called the probability of exceedance (POE) in this paper. Depending on whether the mean parameter shifts toward lower or higher values, the POE is quantified as the area under the density function below or beyond the respective safety threshold

$$\begin{aligned} P(Q_i' < Q_{thres,i}^-) &= \int_{-\infty}^{Q_{thres,i}^-} f_{\mathcal{N}(\mu_{Q_i'},\sigma_{Q_i'})} dq, \\ P(Q_i' > Q_{thres,i}^+) &= \int_{Q_{thres,i}^+}^{\infty} f_{\mathcal{N}(\mu_{Q_i'},\sigma_{Q_i'})} dq, \end{aligned} \tag{14}$$

where $\sigma_{Q_i'} = \sqrt{\mathrm{C}_{Q_i'}}$. The more significant the shift in the input parameter ΔQ_i, the larger the proportion of the posterior distribution beyond the safety interval and the higher the probability of exceedance. Substituting the change definition from Eq. (12) in Eq. (14), the posterior mean $\mu_{Q_i'}$ can be expressed through the parameter change $\mu_{Q_i'} = \mu_{Q_i} + \Delta Q_i$. The posterior covariance $\mathrm{C}_{Q_i'}$, on the other hand, can be calculated based on the Kalman filter from Eq. (6). Therefore, the only unknown on the right side of Eq. (14) is the parameter change ΔQ_i, which can be converted into an equivalent POE (left side of the equation). The most intuitive way to present the mathematical relation is by plotting the POE over the corresponding parameter changes ΔQ_i in so-called POE curves.

Example: Fig. 4 plots the POE curve for the second input parameter Q_2 of the 6-DOF system, which corresponds to the spring stiffness that represents the second floor, see Section 2.4. A parameter shift by −272 MN/m leads to POE of 4.4% (Point A), a parameter change by −513 MN/m leads to a POE of 45.9% (Point B), and a parameter change of −753 MN/m leads to a POE of 93.9% (Point C).

Table 1
Monitored system parameters $\mathbf{Q} = [K_1\ K_2\ K_3]$ of the 6-DOF system.

	K_1 [Mt]	K_2 [Mt]	K_3 [Mt]
Prior PDF	$\mathcal{N}(2000, 400)$	$\mathcal{N}(2000, 400)$	$\mathcal{N}(2000, 400)$
Safety interval $Q^{\pm}_{thres,i}$	[1487, 2513]	[1487, 2513]	[1487, 2513]
User-defined POE	5%	95%	95%
Detectable change Δ_i	−13.6%	−37.7%	−37.7%

3.2. Decision rules to define detectability

In this section, a decision rule is defined based on the POE from Eq. (14), and a framework is introduced to predict the minimum detectable change in system parameters. The probability of exceedance (POE) describes the probability that a monitored input parameter exceeds the safety threshold, and the previous section describes the mathematical relation between the POE and the input parameter changes as continuous POE curves, see Fig. 4 (top). That means that if the system operator is able to prescribe an allowable probability of exceedance, the automated monitoring system can distinguish between the following three system states

$$\begin{aligned}
&\mu_{Q_i'} \approx \mu_{Q_i} \quad \text{if} \quad P(Q_i' < Q^-_{thres,i}) < \mathrm{POE}_i^- \quad \wedge \quad P(Q_i' > Q^+_{thres,i}) < \mathrm{POE}_i^+,\\
&\mu_{Q_i'} < \mu_{Q_i} \quad \text{if} \quad P(Q_i' < Q^-_{thres,i}) \geq \mathrm{POE}_i^-,\\
&\mu_{Q_i'} > \mu_{Q_i} \quad \text{if} \quad P(Q_i' > Q^+_{thres,i}) \geq \mathrm{POE}_i^+,
\end{aligned} \tag{15}$$

where POE_i^+ is the user-defined POE for parameter increases, and POE_i^- for parameter decreases. The limit state is reached if the POE is identical to the user-defined requirements, and the corresponding parameter change is

$$\begin{aligned}
&\Delta Q^-_{min,i} = \Delta Q_i \quad \text{if} \quad P(Q_i' < Q^-_{thres,i}) = \mathrm{POE}_i^-,\\
&\Delta Q^+_{min,i} = \Delta Q_i \quad \text{if} \quad P(Q_i' > Q^+_{thres,i}) = \mathrm{POE}_i^+.
\end{aligned} \tag{16}$$

The parameter changes $\Delta Q^+_{min,i}$ and $\Delta Q^-_{min,i}$ are defined as the minimum detectable changes in this paper, sometimes given as relative changes $\Delta_i = \Delta Q_{min,i}/\mu_{Q_i}$. It is only possible to assess the detectable change after the target values POE_i^- and POE_i^+ have been defined by the user. Although the function is continuous and the POE selection is arbitrary, three main schools of thought will be distinguished in the following to highlight the versatility of the developed framework.

- Highly-critical parameters: A monitored parameter is classified as highly critical, if the consequences of parameter changes are severe. This could be the case if the financial losses are excessive or the safety of human life is at risk, and the automated monitoring system should issue an alarm at the slightest probability that the parameter has changed. In this case, it is in the operator's interest to choose a low value for the target POE, for example 5%. In this case, the posterior's mean value lies within the safety interval when an alarm is issued.
- Non-critical parameters: Not all parameter changes lead to severe consequences and yet, it may be desirable to monitor them. The parameter change may, for example, affect the serviceability of the system or cause discomfort to users. In this case, no alarm should be raised until there is clear evidence that the parameter has changed, and a decision can no longer be postponed. Hence, it is legitimate for operators to choose a higher value for the target POE, i.e. 95%.
- Moderately-critical parameters: The POE can be arbitrarily chosen between zero and one $\mathrm{POE} \in]0, 1[$. In theory, the Gaussian distribution functions of the prior and posterior stretch from $-\infty$ to ∞, and that is why POEs of 0% or 100% are not possible. In some special cases, the system operator might select a POE of 50%, for example, if the parameters are somewhere between highly-critical and non-critical parameters. However, this case deserves special attention and will be discussed in more detail in Section 3.3.

The presented approach is suitable to monitor several parameters at the same time, and since some parameter changes have more severe consequences than others, it may be sensible to select different target POEs for different parameters within the same system.

Example: Table 1 summarizes the detectable damages for the three stiffness values of the 6-DOF system from Section 2.4. The selected POE for stiffness changes on the ground floor is set to 5%, as stiffness decreases could lead to an immediate collapse, so the probability of exceeding the thresholds should be low. The POE for stiffness changes on floor 2 and 3 are set to 95%, as this stiffness value is considered less critical for the integrity of the structure. The results from Table 1 clarify that the minimum detectable stiffness change in floor 2 and 3 are identical. So, detectability does not vary depending on the floor in this case, because the prior and the thresholds are identical. The detectable stiffness change is lower for floor 1, because a lower value for the POE was chosen. Therefore, the developed framework is versatile enough to reflect the importance of different system parameters for the integrity of the structure.

3.3. Optimal detectability

After deriving a framework for the detectable change, a discussion of the limitations and the influencing factors seems in order. Please note that the framework from Section 3.2 cannot be applied if the width of the posterior distribution is significantly wider

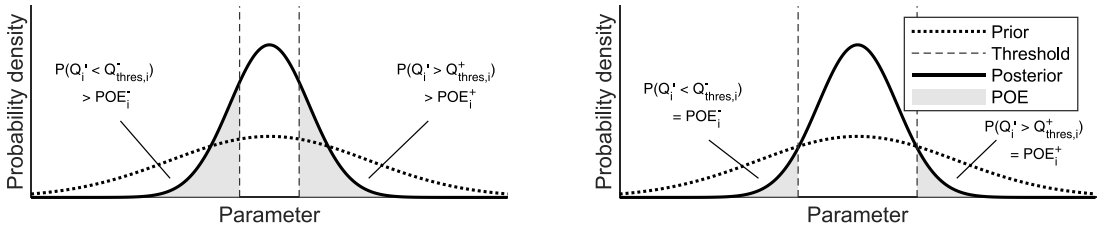

Fig. 5. No decision can be made if the POE is exceeded on both sides of the safety interval (left) or if the POE is equal to the target values on both sides (right). Consequently, the safety interval must satisfy Eq. (18).

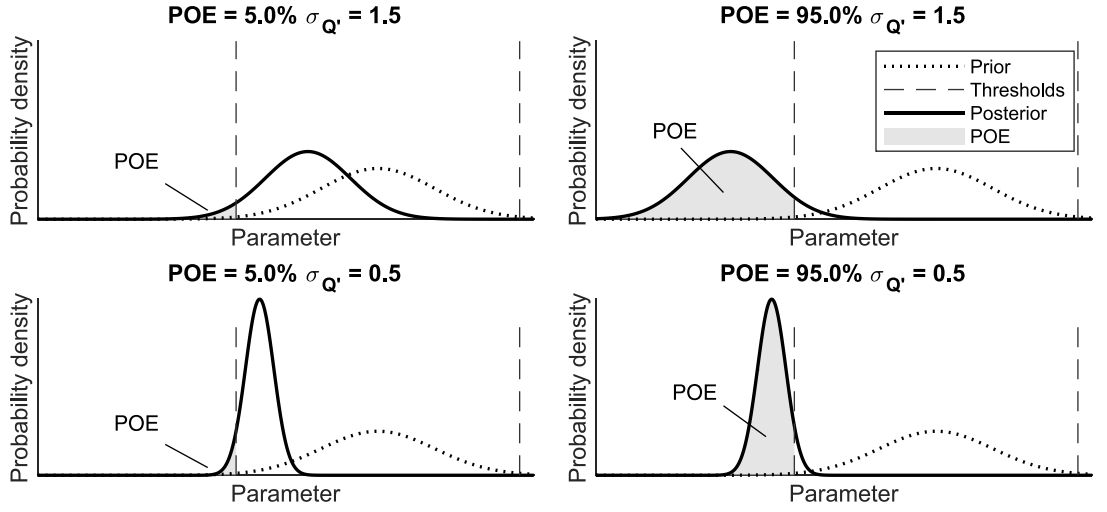

Fig. 6. Assessing the distance measure from Eq. (19) for wide and narrow posteriors, and for highly-critical parameters (left side) and non-critical parameters (right side).

than the safety intervals and a small POE is chosen (highly-critical parameters). As shown in Fig. 5, the user-defined POE is exceeded on either side of the safety interval in this case,

$$P(Q_i' < Q^-_{thres,i}) > \mathrm{POE}_i^- \quad \wedge \quad P(Q_i' > Q^+_{thres,i}) > \mathrm{POE}_i^+, \tag{17}$$

and the three states from Eq. (15) cannot be distinguished. This case occurs if the user selects an inappropriate safety threshold, and the safety interval needs to satisfy the following threshold condition

$$Q^-_{thres,i} < \mu_{Q_i} - k^- \sigma_{Q_i'}, \qquad Q^+_{thres,i} > \mu_{Q_i} + k^+ \sigma_{Q_i'}, \tag{18}$$

which depends on the prior mean μ_{Q_i}, the posterior standard deviation $\sigma_{Q_i'}$, and the user-defined POE at both interval boundaries (POE_i^- and POE_i^+), which can be expressed through the number of standard deviations k, cf. the 68–95–99.7% rule. This indicates that the minimum width of the safety interval depends on the width of the posterior distribution. Therefore, a new distance metric $\mathbf{d}$ is introduced in this section to quantify the degree of "detectability" based on the width of the posterior distribution, or more precisely, its standard deviation

$$\mathbf{d} = \mathrm{diag}(\mathbf{C}_{\mathbf{Q}'})^{1/2}. \tag{19}$$

High detectability is achieved for a parameter Q_i if the posterior standard deviation is small, because then, the distribution is close to the safety threshold with $d_i \to 0$ and the minimum detectable damage $\Delta Q^-_{min,i}$ or $\Delta Q^+_{min,i}$ is small, Fig. 6 (bottom plots). Low detectability $d_i \gg 0$ is given for cases where posterior mean is close to the prior mean or far beyond the safety threshold, see Fig. 6 (top plots). Alternatively, the distance between the posterior mean and the safety threshold could have been chosen, but the distance $\mathbf{d}$ from Eq. (19) is also meaningful if a target POE of 50% is chosen. After substituting the posterior covariance from Eq. (6) into Eq. (19), this resulting equation allows one to identify the influencing factors for optimal change detectability

$$\mathbf{d} = \mathrm{diag}\left(\mathbf{C}_{\mathbf{Q}} - \mathbf{K}\mathbf{C}_{\mathbf{QY}}^T\right)^{1/2}, \qquad \text{where} \qquad \mathbf{K} = \left(\mathbf{C}_{\mathbf{QY}}\left[\mathbf{C}_{\mathbf{Y}} + \mathbf{C}_{\mathbf{E}}\right]^{-1}\right). \tag{20}$$

Table 2
Material properties of the tower model.

	Type	Material	Cross section			
		E [$\frac{\text{MN}}{\text{m}^2}$]	A [m^2]	I [m^4]	EA [MN]	EI [MN m^2]
Pillars	Beam	210 000	1.0	0.146	210 000	30 700
Diagonals	Truss	210 000	0.5	0.146	105 000	30 700

- *Input variance.* A crucial influencing variable is the variance of the input parameters, that is prior knowledge. It can be quantified through the covariance $\mathbf{C_Q}$. More accurate knowledge leads to a lower variance and a narrower posterior distribution, and thus, to a shorter distance d_i for the considered parameter Q_i.
- *Measurement error.* A second influencing factor for the detectability of damage is the measurement error, which is quantified through the covariance $\mathbf{C_E}$. Low-noise sensors, cables, and data acquisition units, or very precise feature estimation methods lead to a low measurement error, a narrower posterior distribution, and a shorter distance d_i.
- *Sensitivity.* Some measurable output quantities respond more rapidly to system changes than others. Mathematically, the sensitivity is captured through the covariance between inputs and outputs $\mathbf{C_{QY}}$ and the output covariance $\mathbf{C_Y}$. A high sensitivity leads to a high covariance $\mathbf{C_{QY}}$ and a small covariance $\mathbf{C_Y}$, and thus, a small distance d_i.

In summary, optimal detectability can be achieved for solid prior knowledge, a small measurement error, and highly sensitive features. Among other applications, the distance d_i is an appropriate measure to verify the signal-to-noise-ratio of measurement equipment, to select the most sensitive features, and to optimize the sensor layout.

3.4. Measurement error

One of the fundamental assumptions of the developed framework is that the measurement error is known, and this section explains how to quantify it based on measurement data. Measurement errors are inevitable and include uncertainties due to measurement noise (noisy sensors, cables, or data acquisition systems), short measurement records, epistemic uncertainties in the feature estimation process, and unknown excitation if stochastic systems are considered. For some monitoring applications, the magnitude of the measurement errors might be known based on the sensor specifications or previous knowledge, but for most monitoring applications, the error has to be estimated based on measurement data. In the following, well-established approaches are categorized into empirical ones and others that are based on perturbation approaches.

Empirical approaches. Fully empirical approaches require a significant amount of data. First, one long measurement is taken and split into hundreds of segments. Secondly, the damage-sensitive features $\mathbf{f} \in \mathbb{R}^{N_f}$ are extracted from each data segment and stored in a feature matrix $\mathbf{F} = [\mathbf{f}_1\ \mathbf{f}_2\ \dots\ \mathbf{f}_N] \in \mathbb{R}^{N_f \times N_s}$ where N_f is the number of features and N_s is the number of data segments. Ultimately, the row means of $\mathbf{F}$ are evaluated and subtracted to obtain the residual matrix $\mathbf{R} = [\mathbf{r}_1\ \mathbf{r}_2 \dots \mathbf{r}_N] \in \mathbb{R}^{N_f \times N_s}$, so the sample covariance can be computed empirically as

$$\mathbf{C}_E = \frac{1}{N-1}\sum_{i=1}^{N} \mathbf{r}_i \mathbf{r}_i^T = \frac{1}{N-1}\mathbf{R}\mathbf{R}^T. \tag{21}$$

Perturbation approaches. This group of methods is able to estimate the sample covariance based on a single measurement record, which reduces the amount of data for the covariance estimation to a single data segment, i.e. $N_s = 1$. Based on perturbation approaches such as the delta-method [36], the uncertainties in the measurement data are quantified, propagated through the feature estimation process, and projected onto the estimated features, with the result being an equivalent covariance matrix $\mathbf{C}_E$. The methods are feature-specific in the sense that each feature requires a different estimation procedure. In the literature, the delta-method has frequently been applied to vibration-based features, such as, frequencies, damping ratios, and mode shapes from operational modal analysis [37,38] or experimental modal analysis [39]. Other authors applied the perturbation approach to residuals that are based on covariance functions [40], or other residuals that are formed in the mathematical subspace of covariance functions [41].

4. Numerical case studies

The developed framework has already been applied to a 6-DOF mass–spring system with a user-defined error covariance. To highlight that the method is equally applicable to static and dynamic measurement quantities, and to demonstrate that the measurement error can be calculated based on data, two more case studies of an offshore tower with inclination sensors and a concrete bridge with vibration sensors are shown in this section.

4.1. Local inclination monitoring of a tower

Jacket-type towers are common support structures for offshore oil platforms or wind turbine towers. Next to storms, extreme waves, and changing operating conditions, mass changes due to marine growth can lead to safety-critical system states. In this numerical study, the mass changes of the support structure are monitored based on inclination sensors, and the goal is to estimate the mass change that can be detected reliably. The tower exhibits a height of 42 m, a width of 30 m at its base, and a width of 12 m

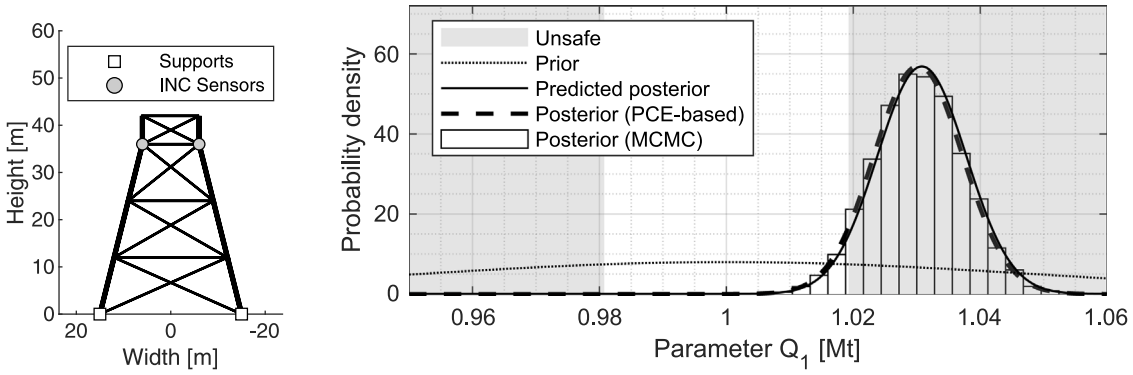

Fig. 7. Jacket-type tower modeled in 2-D (left) and updating result for uniform mass increase (right). The predicted posterior is based on data from the undamaged structure, see Eq. (4), where the other posteriors are based on data from the damaged structure.

Table 3
Monitored system parameters $Q = m$ of the tower.

	m [t]
Prior PDF	$\mathcal{N}(1000, 50)$
Safety interval $Q^{\pm}_{thres,i}$	[981, 1019]
User-defined POE	95%
Detectable change Δ_i	3.09%

at its top, see Fig. 7 (left). The vertical pillars are modeled using 2-D frame elements and the diagonal braces using truss elements, see Table 2. Damage is modeled as a uniform mass change in all submerged elements, with a reference mass of $m = 1000$ t that is applied as point loads to the nodes. For monitoring, two inclination sensors are placed at the joints of the structure, see Fig. 7 (left). In this study, the measurements are directly used as damage-sensitive features and the feature extraction step is skipped. To simulate measurement noise, each reading is superimposed with uniformly distributed noise. In the reference configuration, the mean inclination is 0.026 millidegree and the standard deviation of the measurement error is set to 0.00052 millidegree for each of the two sensors.

(a) Detectable mass change

To assess the detectable mass change, a series of user-inputs have to be made, e.g., the prior distribution of the structural mass, the distribution of the measurement error, the safety thresholds, and the allowable probability of exceedance. First, a normal distribution with a mean of 1000 t and a standard deviation of 50 t is assumed as the prior $\mathbf{Q} \sim \mathcal{N}(1000, 50)$, cf. Table 3. Obviously, the mass experiences no variation but for the computation of displacements and inclinations, the mass is transformed into an equivalent force, and this force may be counteracted by changing tides and varying water buoyancy forces. Secondly, the measurement error is estimated based on data using the empirical approach from Section 3.4. For this purpose, 1000 inclination readings are recorded and stored in a feature matrix, so the covariance matrix can be computed based on Eq. (21) to

$$\mathbf{C}_E = \begin{bmatrix} 0.263 & 0 \\ 0 & 0.266 \end{bmatrix} 10^{-6}. \tag{22}$$

With the prior distribution and the measurement error defined, the standard deviation of the posterior distribution can be predicted based on the Kalman filter. Next, the user-defined probability of exceedance is set to PoE = 95%, and the detectable mass change can be calculated to $\Delta Q = 30.9$ t, which corresponds to a relative mass change of $\Delta_i = 3.09\%$, see Table 3. In other words, if the mass changes by 3.09%, 95% of the posterior distribution should be beyond the safety interval according to the developed framework, as this was the user-defined probability of exceedance.

(b) Validation study

Based on the developed framework, the minimums detectable mass change is calculated to 3.09%. Up until this point, the analysis has been performed based on data from the unchanged state, that is, before the mass changes due to marine growth occurred. Now, the mass is changed for the first time to validate the prediction. For this purpose, a relative change of 3.09% is applied, and if the prediction is accurate, 95% of the posterior distribution should be beyond the safety thresholds, with the result being shown in Fig. 7 (right). The empirical POE of 94.6% is close to the user-defined value of 95%, which shows that the prediction is accurate and concludes the validation study.

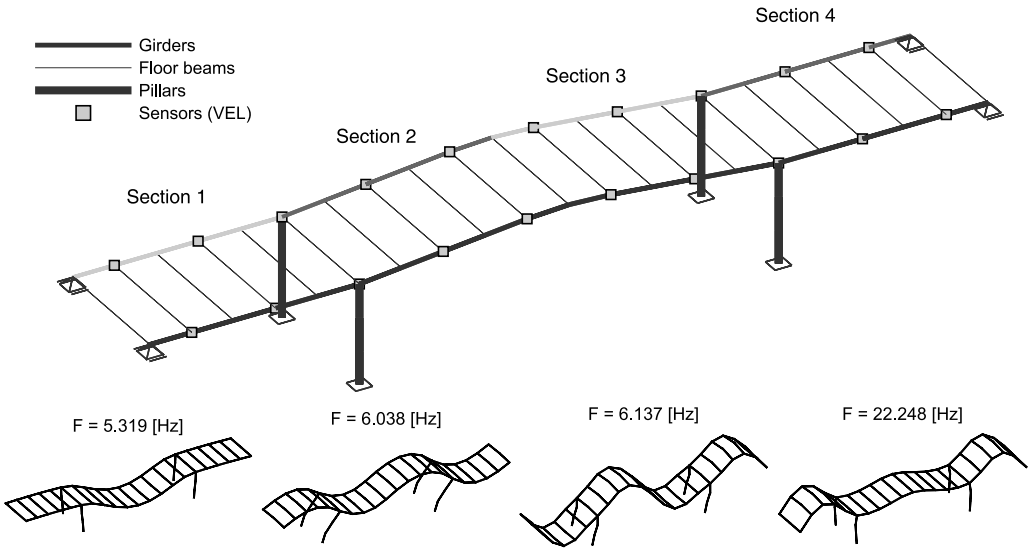

Fig. 8. Model geometry and instrumentation (top) and selected modes of vibration (bottom).

Table 4
Material properties of the bridge model.

Component	Type	Material		Cross section				
		E $[\frac{\mathrm{MN}}{\mathrm{m}^2}]$	m $[\frac{\mathrm{kg}}{\mathrm{m}^3}]$	A $[\mathrm{m}^2]$	I_y $[\mathrm{m}^4]$	I_z $[\mathrm{m}^4]$	G $[\frac{\mathrm{MN}}{\mathrm{m}^2}]$	J $[\mathrm{m}^4]$
Girders	Beam	30000	2500	0.5	0.0417	0.0417	0.0521	$8.4 \cdot 10^{10}$
Floor beams	Beam	30000	2500	0.5	0.0417	0.0417	0.0521	$8.4 \cdot 10^{10}$
Pillars	Beam	30000	2500	1.0	0.0830	0.0830	0.0521	$8.4 \cdot 10^{10}$

(c) Cross-validation

In this section, the validation is repeated but instead of linear Bayesian filters, the Markov Chain Monte Carlo (MCMC) method is applied for updating. The intention is to demonstrate that the prediction is valid regardless of the employed updating method and to cross-validate the results from the PCE-based Kalman filter. For improved efficiency, the PCE model from Section 2 is applied as a surrogate for the physical tower, and a parallelized version of the MCMC algorithm is used, ensuring a faster convergence [42]. The results are also shown in Fig. 7 (right) through white histograms to clarify that this procedure solves the updating problem through sampling instead of analytical operations. The differences between PCE-based Kalman filter and the MCMC method are insignificant, and the MCMC-based POE of 94.2% is very close to the theoretical value of 95%.

4.2. Global modal parameter monitoring of a bridge

Bridges are critical components in lifeline infrastructure that are exposes to various natural hazards, e.g., floods, storms, earthquakes, or impacts of any sort. Global vibration-based approaches based on natural frequencies and mode shapes are often criticized because of their low sensitivity to small and local damages [43]. Hence, it is particularly interesting to predictively assess which damages can or cannot be detected, and to calculate the detectable change. In the following, the detectable damage will be calculated for a three-span bridge with clamped pillars, and abutments that allow the bridge to move in the longitudinal direction. Longitudinal girders, floor beams, and pillars are modeled through concrete beam elements with the properties from Table 4. Fig. 8 visualizes the geometry and clarifies that all following studies focus on the material properties of one longitudinal girder, which is divided into four sections. The excitation is modeled as white noise and applied to all 450 degrees of freedom. Twenty uni-axial vibration sensors measure the velocities in the vertical direction. To simulate a very noise environment, the structural vibration signal is superimposed with uniformly distributed noise with a maximum magnitude of 3.5-times the standard deviation of the structural signal. In contrast to the previous study, the system response is not monitored directly but natural frequencies and mode shapes of the first four modes of vibration (in the vertical direction) are extracted and treated as system observations.

(a) Detectable stiffness changes

In this study, the natural frequencies and mode shapes are estimated based on operational modal analysis, or more precisely, based on covariance-driven subspace system identification (SSI-Cov) [44]. In combination with the perturbation approach described in Section 3.4, this method allows one to quantify the uncertainties in the natural frequencies and mode shapes based on a single

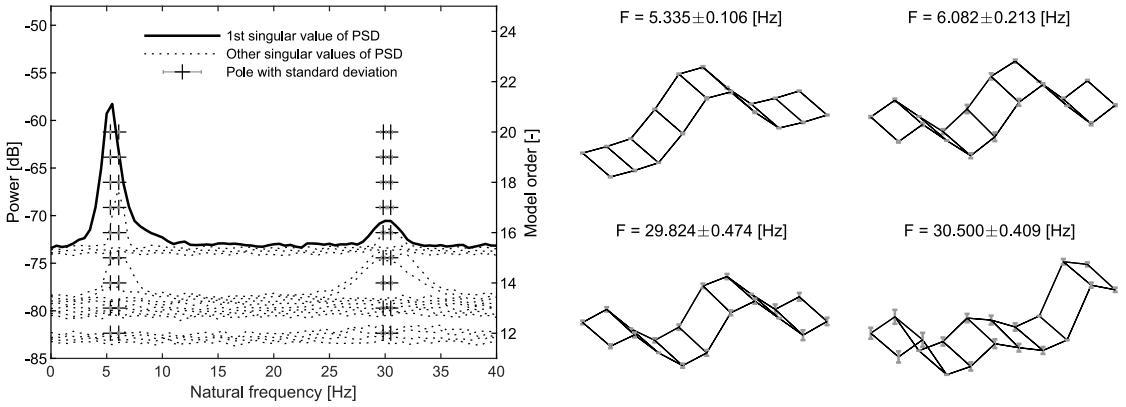

Fig. 9. Natural frequencies in the stabilization diagram (left) and corresponding mode shapes at the sensor locations (right) including error bars for the measurement error with a magnitude equal to three times the standard deviation.

Table 5
Monitored system parameters $\mathbf{Q} = [Q_1\ Q_2\ Q_3\ Q_4]$ of the bridge.

	Q_1	Q_2	Q_3	Q_4
Prior PDF	$\mathcal{N}(1.0, 0.1)$	$\mathcal{N}(1.0, 0.1)$	$\mathcal{N}(1.0, 0.1)$	$\mathcal{N}(1.0, 0.1)$
Safety interval $Q^{\pm}_{thres,i}$	[0.77, 1.23]	[0.77, 1.23]	[0.77, 1.23]	[0.77, 1.23]
User-defined POE	5%	5%	5%	5%
Posterior covariance $C_{Q'_i}$	$0.130 \cdot 10^{-3}$	$0.112 \cdot 10^{-3}$	$0.164 \cdot 10^{-3}$	$0.058 \cdot 10^{-3}$
Detectable change Δ_i	−20.8%	−20.9%	−20.5%	−21.5%

measurement record [37,38] with the stabilization diagram being shown in Fig. 9 (left). A data fusion technique is employed to merge the modal parameters from varying system orders into a single frequency and mode shape for each mode, while considering the estimation errors [45]. To indicate the uncertainties, Fig. 9 (right) shows error bars with a magnitude equal to three times the standard deviation. In total, 80 system observations are monitored and displayed, i.e., four frequencies and 76 mode shapes coordinates. In operational modal analysis, mode shapes are non-unique in the sense that real or complex-valued entries may differ after a repeated estimation. For normalization, the maximum mode shape coordinate is scaled to unit-displacement, making one mode shape component insensitive to damage and reducing the number of damage-sensitive mode shape components from $4{\times}20 = 80$ to 76.

As described above, the monitored system inputs are the E-Moduli of the four girder sections, so $[E_1\ E_2\ E_3\ E_4]^T$. Instead of using a stiffness parameter directly, each E-Modulus E_i is pre-multiplied by a random variable and this variable vector $\mathbf{Q} = [Q_1, Q_2, Q_3, Q_4]^T$ is used as the monitored system input. As shown in Table 5, the prior PDF of each Q_i is defined by the mean value of one and the standard deviation of 0.1, so $Q_i \sim \mathcal{N}(1.0, 0.1)$. The table also shows the user-defined safety interval for each variable and the user-defined probability of exceedance of 5%.

With the priors and the measurement error being defined, the detectable change in each girder section can be calculated to approximately −21%, see Table 5. On close inspection of the table, it can be appreciated that the posterior variances vary slightly for each parameter; however, the differences are insignificant, especially in comparison to the width of the safety interval, leading to an almost identical detectable change for each parameter.

(b) Validation for single-damage scenarios

For validation, the stiffness in Section 3 of the main girder is reduced by the detectable change of −20.5%, see Table 5. If the prediction of the detectable damage is correct, 5% of the posterior distribution should be beyond the safety threshold, as this was the user-defined POE. By looking at the validation plot in Fig. 10 (left), it can be appreciated that the distribution for the changed parameter (dashed line) moves beyond the safety thresholds and approximates the predicted distribution (solid line), while all other parameter distributions stay within the safety interval. For parameter Q_3, the POE is 4.4%, which is very close to the target POE of 5%. For unchanged parameters, the distributions are similar to the prior (dotted line), and some insignificant deviations can be noticed. A thorough analysis, based on Sobol indices [46], reveals that the inaccuracies are due sensitivity issues, as changes in structural parameter cause less significant changes in modal parameters. More on this follows in the discussion in Section 4.3.

(c) Validation for multiple-damage scenarios

The division of the girder into four damage zones appears arbitrary, and it cannot be guaranteed that damage is restricted to one girder section in practice, cf. Fig. 8. Therefore, an interesting research question is whether the predicted detectable damage

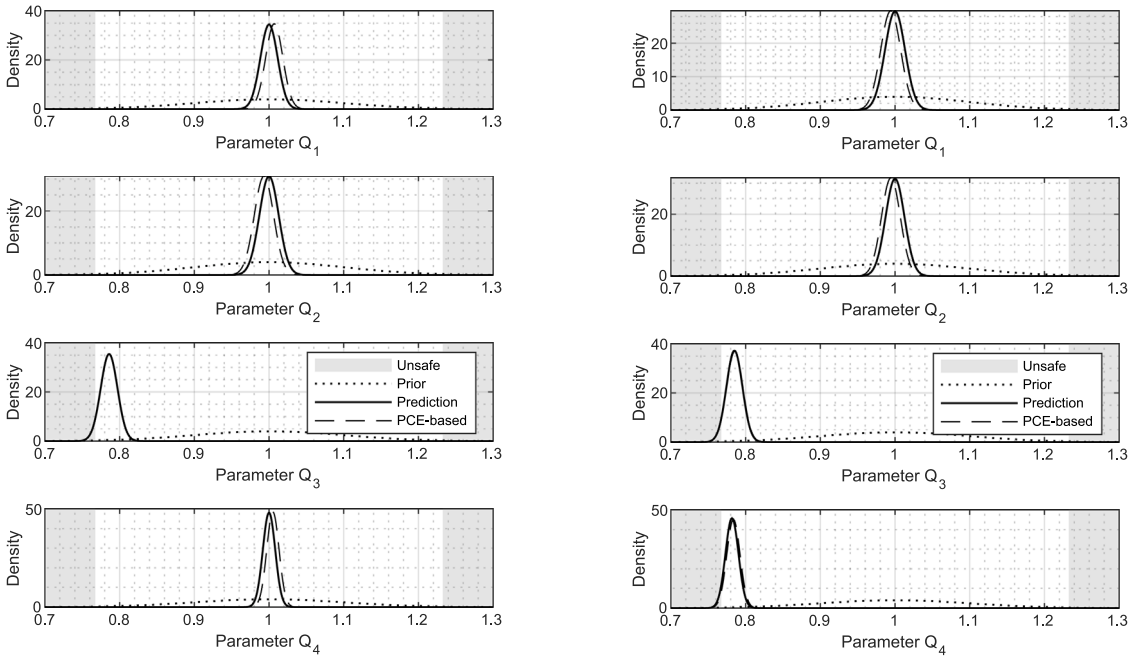

Fig. 10. Validation results for a single-damage scenario with damage in parameter Q_3 (left side) and for a multiple-damage scenario with damage in parameters Q_3 and Q_4 (right side).

is also valid for scenarios, where changes occur in multiple input parameters at the same time. To analyze this, the third and fourth parameters are changed by the detectable change from Table 5, and the validation procedure is rerun. The results in Fig. 10 (right) demonstrate that the prior mean value of both parameters shifts by the detectable change, and that the empirical POE of 4.1% and 2.0% are close to the theoretical value of 5%. Again, the inaccuracies are due to the low sensitivity of the employed damage-sensitive features, which is discussed in the subsequent section. It appears that no modifications have to be made to the theory, as the predictions are also valid for multiple-damage scenarios.

4.3. Discussion

The numerical case studies in this paper demonstrated that the detectable changes can be predicted based on linear Bayesian filters. While the developed framework appears to deliver highly accurate results for the 6-DOF system and the offshore tower, the bridge case study exhibits minor inaccuracies in the prediction. The following discussion highlights that inaccuracies are not only due to the limitations of the developed approach but also the limitation of Bayesian updating in general.

The developed method is based upon linear Bayesian filters but this does not mean that the system observations have to be linear functions of the system parameters. For example, the natural frequencies of the 6-DOF system are non-linear functions of the stiffness parameters, especially for large parameter changes up to 37.7% (see Fig. 4), and yet, the developed framework delivered highly accurate results based on linear filters. This finding is substantiated by similar studies in the literature on PCE-based Kalman filters [33,47]. An important aspect is that only for linear Bayesian filters, the posterior covariance is independent of the observation, cf. Eq (4), meaning the posterior can be analytically evaluated based on data from the unchanged state. Moreover, the posterior mean and the covariance matrix can be computed without sampling, which significantly increased the computation speed in comparison to traditional methods such as MCMC methods. However, one of the downsides of linear Bayesian filters is that large shifts in the system parameter or significant non-linearities in the system may distort the Gaussian assumption and lead to slight inaccuracies in the prediction of the detectable damage.

The assumption of Gaussianity should also be clarified, as the PCE-based Kalman filter is also capable of updating non-Gaussian random variables. The Gaussian assumption for the prior and the posterior was essential for the change definition from Eq. (12) as the shift in the mean values. If the observations are highly non-linear functions of the system parameters, the posterior random variable is no longer Gaussian and asymmetries may occur in the posterior distribution, leading to inaccuracies in the prediction.

Ultimately, sensitivity issues can bias the accuracy in validation studies. Sensitivity issues arise if large changes in system parameters lead to insignificant changes in the observed system outputs, as it is the case for the bridge case study. An appropriate tool to evaluate the sensitivity is the calculation of partial variances through Sobol indices [46], which quantify the contribution of an observation to the variance in the updating parameters. By applying them to the bridge in Section 4.2, it can be concluded that mode shapes are highly sensitive to changes in Section 3, followed by Section 4, but they are not very sensitive to changes in Sections 1 and 2. That means that changes in Section 4 are more challenging to identify due to the limited sensitivity, and this is one of the basic limitation of system identification, regardless of the employed method.

5. Conclusion

This paper develops an approach to determine the detectable change for linear Bayesian filters. The main contribution is the statistical framework that relates changes in observations to the changes in system parameters and the probability of exceeding a safety threshold through so-called probability of exceedance curves. This enables system operators to choose an arbitrary probability of exceedance, which can subsequently be translated in a corresponding ‘‘minimum detectable change’’ in structural or material parameters. The introduced concept based on the probability of exceedance are reminiscent of approaches related to the probability of detection and the probability of localization. However, these terms are intentionally avoided in this paper, due to the fundamental discrepancies between hypothesis testing based on frequentist and Bayesian methods. The resulting quantity, the minimum detectable change, is a physically meaningful metric to assess monitoring systems. For example, it could be used for the following purposes:

- Investment justification. If the detectable changes are unreasonably high, it is not possible to detect damage based on automated monitoring systems. In that case, the investment is not justified, and other inspections techniques should be considered.
- Feature selection. With reference to the presented case studies, engineers could assess whether it makes the most sense to measure inclinations, vibrations, or to extract natural frequencies, or mode shapes, as the most sensitive features will lead to a high detectability (a small minimum detectable change).
- Sensor selection. Some sensors and hardware components exhibit a lower signal-to-noise-ratio than others, leading to higher detectability (a lower minimum detectable change). Hence the minimum detectable change assesses the signal quality in a physically meaningful way.
- Sensor placement optimization. Some sensor layouts lead to a higher detectability than others (quantified through a low value for the minimum detectable change) and these layouts should be preferred.
- Optimized maintenance. If material-specific degradation functions are available, the developed approach can be employed to estimate probable failure times, and all associate costs throughout the life cycle of a structure.

The approach has to be combined with a suitable method to estimate the measurement error, i.e., the uncertainty in the system observations. To demonstrate this, the paper introduces three case studies of varying complexity. The first study is a 6-DOF mass-and-spring system, where the detectable change in lumped masses and spring stiffness values is determined based on changes in numerical modal frequencies, and the measurement error is predefined by the authors for reproducibility. The second study evaluates the detectable mass change due to marine growth on a jacked-type offshore tower, typically used for wind farms or oil platforms. The tower is monitored with inclination sensors, and the synthetically generated measurement error is quantified based on an approach that could be universally applied to any kind of measurement. The third study evaluates the detectable stiffness change on the main girder of a concrete bridge due to seismic damage. The study employs operational modal analysis to experimentally determine natural frequencies and mode shapes based on vibration measurements, and to evaluate the measurement error based on a single measurement record from the undamaged structure. Therefore, the developed method is also applicable if the amount of data from the unchanged state is limited.

One of the distinguishing features of the developed method is that no data from the changed state is required to assess the detectability of changes, as the posterior covariance can be calculated based on Kalman filters, and it is independent of the observation in the changed state. Such ‘‘predictive’’ methods are rare and have only been reported for damage detection and localization. Bayesian methods not only allow for damage quantification as well, but they perform the damage detection, localization, and quantification in one step. In this paper, a framework was introduced to assess the parameter changes based on Bayesian methods, which, following the train of thought from above, corresponds to an assessment of the quantifiability of damage. However, the problems related to damage localization remained unaddressed, and no comprehensive framework was introduced for a combined damage localization and quantification. This will be the subject of future research studies.

Declaration of competing interest

The authors declare that they have no known competing financial interests or personal relationships that could have appeared to influence the work reported in this paper.

Data availability

Data will be made available on request.

Acknowledgments

This research project is funded by dtec.bw – Digitalization and Technology Research Center of the Bundeswehr which we gratefully acknowledge. dtec.bw is funded by the European Union – NextGenerationEU. Special thanks go to Michael Döhler from the French National Institute for Research in Digital Science and Technology (Inria) in Rennes for providing the Matlab code for the modal parameter estimation and uncertainty quantification. The application of the functional Kalman Filter was made possible by the implementation of the Matlab toolbox SGLib. Special thanks also go to Noemi Friedman from the SZTAKI Institute in Budapest who provided the most recent SGLib functions.

References

[1] C. Farrar, K. Worden, Structural Health Monitoring: A Machine Learning Perspective, Wiley, Oxford, United Kingdom, 2012.
[2] A. Rytter, Vibrational Based Inspection of Civil Engineering Structures (Ph.D. thesis), Aalborg University, Aalborg, 1993.
[3] R.N. Coppolino, S.N. Rubin, Detectability of structural failures in offshore platforms by ambient vibration monitoring, in: Proceedings of the OTC - 12th Offshore Technology Conference, Houston, United States, May, 1980.
[4] A. Cabboi, C. Gentile, A. Saisi, From continuous vibration monitoring to FEM-based damage assessment: Application on a stone-masonry tower, Constr. Build. Mater. 156 (2017) 252–265.
[5] N. Cavalagli, G. Comanducci, F. Ubertini, Earthquake-induced damage detection in a monumental masonry bell-tower using long-term dynamic monitoring data, J. Earthq. Eng. 22 (2018) 96–119.
[6] C.R. Farrar, P.J. Cornwell, S.W. Doebling, M.B. Prime, Structural Health Monitoring Studies of the Alamosa Canyon and I-40 Bridges, Tech. rep., Los Alamos National Laboratories, Los Alamos, United States, 2000.
[7] A.P. Berens, NDE Reliability Data Analysis–Metals Handbook, ASM International, United States, 1989.
[8] MIL-HDBK, Department of Defense Handbook, Nondestructive Evaluation System Reliability Assessment, Tech. rep., Department of Defense, Washington, United States, 2009.
[9] ASTME-3023, Standard Practice for Probability of Detection Analysis for A-Hat Versus a Data, Tech. rep., ASTM International, West Conshohocken, United States, 2015.
[10] A. Mendler, M. Döhler, C.E. Ventura, A reliability-based approach to determine the minimum detectable damage for statistical damage detection, Mech. Syst. Signal Process. 154 (2021) 107561.
[11] A. Mendler, M. Döhler, C.E. Ventura, L. Mevel, Localizability of damage with statistical tests and sensitivity-based parameter clusters, Mech. Syst. Signal Process. (2023) submitted for publication.
[12] E. Simoen, G. De Roeck, G. Lombaert, Dealing with uncertainty in model updating for damage assessment: A review, Mech. Syst. Signal Process. 56–57 (2015) 123–149.
[13] I. Behmanesh, B. Moaveni, Probabilistic identification of simulated damage on the dowling hall footbridge through Bayesian finite element model updating, Struct. Control Health Monit. 22 (3) (2015) 463–483.
[14] A. Kamariotis, E. Chatzi, D. Straub, Value of information from vibration-based structural health monitoring extracted via Bayesian model updating, Mech. Syst. Signal Process. 166 (2022) 108465.
[15] J.K. Kruschke, Doing Bayesian Data Analysis. A Tutorial with R, JAGS, and Stan, Academic Press, Elsevier, London, United Kingdom, 2015.
[16] B.V. Rosić, J. Sýkora, O. Pajonk, A. Kučerová, H.G. Matthies, Comparison of numerical approaches to Bayesian updating, Tech. Rep. 2014–10, Institute of Scientific Computing Carl-Friedrich-Gauss-Faculty, Technical University of Braunschweig, Braunschweig, Germany, 2014.
[17] H.G. Matthies, E. Zander, B.V. Rosić, A. Litvinenko, O. Pajonk, Inverse problems in a Bayesian setting, in: A. Ibrahimbegovic (Ed.), Computational Methods for Solids and Fluids: Multiscale Analysis, Probability Aspects and Model Reduction, Vol. 41, Springer, Cham, 2016, pp. 245–286.
[18] H. Matthies, A. Litvinenko, B.V. Rosić, E. Zander, Parameter estimation via conditional expectation: a Bayesian inversion, Adv. Model. Simul. Eng. Sci. 3 (1) (2016) 1–27.
[19] D. Xiu, Numerical Methods for Stochastic Computations: A Spectral Method Approach, Princeton University Press, Princeton, United States, 2010.
[20] B. Kurent, N. Friedman, W.K. Ao, B. Brank, Bayesian updating of tall timber building model using modal data, Eng. Struct. 266 (2022) 114570.
[21] G. Sevieri, A. de Falco, Dynamic structural health monitoring for concrete gravity dams based on the Bayesian inference, J. Civ. Struct. Health Monit. 10 (2) (2020) 235–250.
[22] G. Sevieri, M. Andreini, A. De Falco, H.G. Matthies, Concrete gravity dams model parameters updating using static measurements, Eng. Struct. 196 (2019) 109231.
[23] F. Marsili, P. Croce, N. Friedman, P. Formichi, F. Landi, Seismic reliability assessment of a concrete water tank based on the Bayesian updating of the finite element model, ASCE-ASME J. Risk Uncertain. Eng. Syst. B 3 (2) (2017) 021004.
[24] B.V. Rosić, A. Litvinenko, O. Pajonk, H.G. Matthies, Sampling-free linear Bayesian update of polynomial chaos representations, J. Comput. Phys. 231 (17) (2012) 5761–5787.
[25] O. Pajonk, B.V. Rosić, A. Litvinenko, H.G. Matthies, Deterministic Filter for Non-Gaussian Bayesian Estimation, Tech. Rep. 2011–04, Institute of Scientific Computing Carl-Friedrich-Gauss-Faculty, Technical University of Braunschweig, Braunschweig, Germany, 2011.
[26] T. Wu, B.V. Rosić, L. De Lorenzis, H.G. Matthies, Parameter identification for phase-field modeling of fracture: A Bayesian approach with sampling-free update, Comput. Mech. 67 (2021) 435–453.
[27] E. Adeli, B.V. Rosić, H.G. Matthies, S. Reinstädler, Effect of load path on parameter identification for plasticity models using Bayesian methods, in: M. D'Elia, M. Gunzburger, G. Rozza (Eds.), Quantification of Uncertainty: Improving Efficiency and Technology: QUIET Selected Contributions, Springer International Publishing, Cham, 2020, pp. 1–13.
[28] E. Adeli, B.V. Rosić, H.G. Matthies, S. Reinstädler, D. Dinkler, Comparison of Bayesian methods on parameter identification for a viscoplastic model with damage, Probab. Eng. Mech. 62 (2020) 103083.
[29] J. Waeytens, B. Rosić, P.-E. Charbonnel, E. Merliot, D. Siegert, X. Chapeleau, R. Vidal, V. le Corvec, L.-M. Cottineau, Model updating techniques for damage detection in concrete beam using optical fiber strain measurement device, Eng. Struct. 129 (2016) 2–10.
[30] A. Litvinenko, H.G. Matthies, Inverse Problems and Uncertainty Quantification, Tech. Rep. 2013–04, Institute of Scientific Computing Carl-Friedrich-Gauss-Faculty, Technical University of Braunschweig, Braunschweig, Germany, 2011.
[31] G. Evensen, The ensemble Kalman filter for combined state and parameter estimation, IEEE Control Syst. Mag. 29 (3) (2009) 83–104.
[32] N. Friedman, C. Zoccarato, E. Zander, H.G. Matthies, Parameter identification based on conditional expectation, in: J. Chiachío-Ruano, M. Chiachío-Ruano, S. Sankararaman (Eds.), Bayesian Inverse Problems: Fundamentals and Engineering Applications, CRC Press, Oxford, 2021, Ch. 4.
[33] B.V. Rosić, A. Kučerová, J. Sýkora, O. Pajonk, A. Litvinenko, H.G. Matthies, Parameter identification in a probabilistic setting, Eng. Struct. 50 (2013) 179–196.
[34] N. Wiener, The homogeneous chaos, Amer. J. Math. 60 (4) (1938) 897–936.
[35] H.G. Matthies, Uncertainty quantification with stochastic finite elements, in: E. Stein, R. de Borst, T. Hughes (Eds.), Encyclopaedia of Computational Mechanics, Wiley, Cham, 2007.
[36] G. Casella, R.L. Berger, Statistical Inference, Duxbury, Pacific Grove, California, 2002.
[37] E. Reynders, R. Pintelon, G. De Roeck, Uncertainty bounds on modal parameters obtained from stochastic subspace identification, Mech. Syst. Signal Process. 22 (4) (2008) 948–969.
[38] M. Döhler, L. Mevel, Efficient multi-order uncertainty computation for stochastic subspace identification, Mech. Syst. Signal Process. 38 (2) (2013) 346–366.
[39] P. Mellinger, M. Döhler, L. Mevel, Variance estimation of modal parameters from output-only and input/output subspace-based system identification, J. Sound Vib. 379 (2016) 1–27.
[40] S. Greś, M. Döhler, P. Andersen, L. Mevel, Subspace-based mahalanobis damage detection robust to changes in excitation covariance, Struct. Control Health Monit. (2021) e2760.
[41] M. Basseville, M. Abdelghani, A. Benveniste, Subspace-based fault detection algorithms for vibration monitoring, Automatica 36 (1) (2000) 101–109.

[42] F. Landi, F. Marsili, N. Friedman, P. Croce, gPCE-based stochastic inverse methods: A benchmark study from a civil engineer's perspective, Infrastructures 6 (11) (2021).
[43] J.M.W. Brownjohn, A.D. Stefano, Y.-L. Xu, H. Wenzel, A.E. Aktan, Vibration-based monitoring of civil infrastructure: Challenges and successes, J. Civ. Struct. Health Monit. 1 (3–4) (2011) 79–95.
[44] P. van Overschee, B. de Moor, Subspace Identification for Linear Systems: Theory, Implementation, Application, Kluwer Academic Publishers, Boston/London/Dordrecht, 1995.
[45] M. Döhler, P. Andersen, L. Mevel, Variance computation of modal parameter estimates from UPC subspace identification, in: Proceedings of the IOMAC–7th International Operational Modal Analysis Conference, Ingolstadt, 2017.
[46] B. Sudret, Global sensitivity analysis using polynomial chaos expansions, Reliab. Eng. Syst. Saf. 93 (7) (2008) 964–979.
[47] O.G. Ernst, B. Sprungk, H.-J. Starkloff, Bayesian inverse problems and Kalman filters, in: Extraction of Quantifiable Information from Complex Systems, in: Lecture Notes in Computational Science and Engineering, vol. 102, Springer, 2014, pp. 133–159.